Applied Catalysis B: Environment and Energy 350 (2024) 123943

Contents lists available at ScienceDirect

Applied Catalysis B: Environment and Energy

journal homepage: www.elsevier.com/locate/apcatb

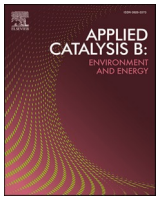

Macrocycle-on-COF photocatalyst constructed by in-situ linker exchange for efficient photocatalytic CO_2 cycloaddition

Xiaojuan Li [a,1], Xinxin Niu [a,1], Peng Fu [a], Yaru Song [a], Enbing Zhang [a], Yanfeng Dang [a,*], Jing Yan [a,*], Guangyuan Feng [a,*], Shengbin Lei [a,b,**], Wenping Hu [a]

[a] Key Laboratory of Organic Integrated Circuit, Ministry of Education &Tianjin Key Laboratory of Molecular Optoelectronic Sciences, Department of Chemistry, School of Science, Tianjin University & Collaborative Innovation Center of Chemical Science and Engineering, Tianjin 300072, China
[b] School of Chemistry and Chemical Engineering, Lanzhou Jiaotong University, Lanzhou 730070, China

ARTICLE INFO

Keywords:
Covalent organic frameworks
Core-shell hybrids
Linker exchange
Macrocycle
Photocatalytic CO_2 cycloaddition

ABSTRACT

Functionalizing macrocycle with gas capture and catalytic ability onto covalent organic frameworks (COFs) can generate hierarchical porous materials with enhanced properties, while the challenge is how to improve full utilization of the active sites and maintain the crystallinity of the parent framework. Herein, we developed a "Macrocycle-on-COF" strategy by partial in-situ linker exchange to gain core-shell hybrids containing hierarchical pores. We demonstrated that the macrocycle-on-COF with functionalized pillar[5]arene have a profound effect on highly CO_2 adsorption and abundant active sites. The photoelectrical measurement showed that the macrocycle-on-COF was an excellent photocatalyst with fast photoresponse and superior charge separation efficiency. With the assistance of light, the functionalized OH-P[5]-on-COF achieves efficient photocatalytic CO_2 cycloaddition reaction under ambient conditions (20 °C and 1 atm), in which a 99% conversion can be achieved within 3 h and the performance is superior compared to previously reported COFs. This study presents the first example of using COFs as photocatalysts for photocatalytic CO_2 cycloaddition reaction under ambient conditions.

1. Introduction

Covalent organic frameworks (COFs) are an emerging class of crystalline porous material that feature tunable band gaps, large conjugation structure and outstanding visible light absorbance, have been proven to be an excellent photocatalyst for various photocatalytic reactions, including water splitting, CO_2 reduction, pollution degradation, and organic transformations [1–6]. However, limited choice of building blocks, fewer active sites, onefold pore environment and components greatly restrict the photochemical performance, particularly with respect to the heterogeneous reaction. For instance, in CO_2 cycloaddition reaction, the gas-liquid-solid phase has relatively large mass transfer resistance and difficulties in reaching the active sites, leading to the necessary reaction condition with high pressure or/and high temperature [7–9]. The preparation of hierarchical core-shell COFs with both micropores and mesoporous by a rational structure design is an attractive route to solve this problem. In hierarchical porous materials, the sub-nanopores and micropores mainly accommodate gas molecules and active sites, and the mesoporous as channels for promoting the accessibility of liquid phase reactants to active sites, the unique hierarchical structure favors to minimize the diffusion barriers and shorten the mass transfer pathways [10–13]. What's more, the core-shell structure ensures the full utilization of active sites and rapid mass transfer/diffusion of reactants [14,15]. However, due to the fast reaction characteristics during COFs synthesis, which results in rapid self-coagulation and precipitation of COFs species, leading to formation of irregular structure and morphology [16–18]. Core-shell hybrids consisting of two different COFs with high crystallinity, precise structure and hierarchical pores are still rare.

On the other hand, effectively capturing and transforming CO_2 into value-added chemicals have become essential but remain a challenging task. The cycloaddition of CO_2 with epoxides to form cyclic carbonates is very promising, due to its 100% atom economy and wide applications. The new findings suggest that introducing active sites (Lewis acids,

* Corresponding authors.
** Corresponding author at: Key Laboratory of Organic Integrated Circuit, Ministry of Education &Tianjin Key Laboratory of Molecular Optoelectronic Sciences, Department of Chemistry, School of Science, Tianjin University & Collaborative Innovation Center of Chemical Science and Engineering, Tianjin 300072, China.
E-mail addresses: yanfeng.dang@tju.edu.cn (Y. Dang), jingyan@tju.edu.cn (J. Yan), fengguangyuan@tju.edu.cn (G. Feng), shengbin.lei@tju.edu.cn (S. Lei).
[1] These authors contributed equally to this work.

https://doi.org/10.1016/j.apcatb.2024.123943
Received 7 January 2024; Received in revised form 27 February 2024; Accepted 9 March 2024
Available online 11 March 2024

bases, hydrogen-bond donors, nucleophilic anions, etc.) into the COFs skeleton can achieve efficient metal-free catalysts [19–22]. Given the good affinity of pillar[5]arene toward CO_2 and the easy introduction of polyhydroxyl groups at the edge of the pillar[5]arene [23–26], which can help to capture and activate CO_2, introducing pillar[5]arene into core-shell COFs may result in efficient catalysts for cycloaddition of CO_2.

The linker exchange strategy is an effective approach to realize COF-to-COF transformation via in-situ replacing the linker of the former with a new linker, which has been extended to transformation between COFs with different linkages and dimensionality [11,14,27–31]. The realization of linker exchange is based on the reversibility of covalent bonding, which can be enabled by applying dynamic covalent chemistry (DCC) [27,32,33]. To obtain high conversion efficiency, previous studies usually used smaller or similar linkers to replace the former linkers to ensure the exchange reactions to occur [28,30,34]. Herein, to prepare core-shell COFs with pillar[5]arene by partial linker exchange, our "Macrocycle-on-COF" strategy goes in the opposite direction, in which the large pillar[5]arene linker (P[5]A) was used to replace the terphenyl linker (TPDAe) (Scheme 1).

And to develop effective catalytic systems to achieve metal-free, solvent-free and under ambient conditions, we further functionalized the P[5]-on-COF to obtain hydroxylated OH-P[5]-on-COF that with hydrogen-bond donors. Excitingly, the functionalized OH-P[5]-on-COF achieves efficient photocatalytic CO_2 cycloaddition reaction under ambient conditions (20 °C and 1 atm), in which a 99% conversion can be achieved within 3 h and the performance is superior compared to previously reported COFs.

2. Experimental section

2.1. Preparation of TT-COF

The TT-COF were carried out by a Schiff-base condensation reaction. A 10 mL Pyrex tube. was charged with 4,4',4'',4'''-(pyrene-1,3,6,8-tetrayl)tetraaniline (TAPPy) (11.3 mg, 0.02 mmol), 2′,5′-bis(2-(2-methoxyethoxy)ethoxy)-4,4''-dimethyl-1,1′:4′,1''-terphenyl (TPDAe) (20.9 mg, 0.04 mmol) and 1 mL mixed solvent o-dichlorobenzene/ethanol (1:1 v/v). The resulting mixture was sonicated 10 min before adding 6 M acetic acid (0.2 mL) to the solution. Then Pyrex tube was degassed through three freeze-pump-thaw cycles before sealing under vacuum. Upon warming to room temperature, the tube was heated at 120 °C for 3 days. After cooling to room temperature, the resulted yellow solid was isolated by filtration, washed sequentially with tetrahydrofuran (THF) and acetone, and dried under vacuum overnight to afford TT-COF as a yellow powder.

2.2. Preparation of P[5]-on-COF

The P[5]-on-COF was obtained via partial in-situ linker exchange. A 10 mL Pyrex tube. was charged with TT-COF (10 mg), P[5]A (11 mg, 33 mg, 66 mg, 111 mg for 1 eq., 3 eq., 6 eq., 10 eq., respectively) and 1 mL ethanol as solvent. The resulting mixture was sonicated 10 min before adding 6 M acetic acid (0.2 mL) to the solution. Then Pyrex tube was degassed through three freeze-pump-thaw cycles before sealing under vacuum. Upon warming to room temperature, the tube was heated at 120 °C for 3 days. After cooling to room temperature, the resulted yellow solid was isolated by filtration, washed sequentially with THF and acetone, and dried under vacuum overnight to afford P[5]-on-COF as a yellow powder.

2.3. Photocatalytic experiments

In general, a mixture of catalyst (1.5 mg), tetra-butylammonium bromide (TBAB, 0.0125 mmol) and epoxides (0.25 mmol) were placed into a 10 mL sealed quartz glass tube. The tube was purged with a balloon filled with pure CO_2 for more than 10 min to remove the air and vapor in the tube. The catalytic cycloaddition reaction was carried out under light irradiation with a LED lamp at 20°C and 1 atm. After the reaction, the products were extracted with $CDCl_3$ and analyzed by ^1H NMR spectroscopy. And the catalysts were washed with ethanol and dichloromethane, collected by centrifugation and dried for catalyst recycling test.

3. Results and discussion

3.1. Characterizations of macrocycle-on-COF

In order to obtain core-shell macrocycle-on-COF containing pillar[5]arene, the functionalized pillar[5]arene (P[5]A) was synthesized according to reported procedure (Scheme S2), and the precise structure

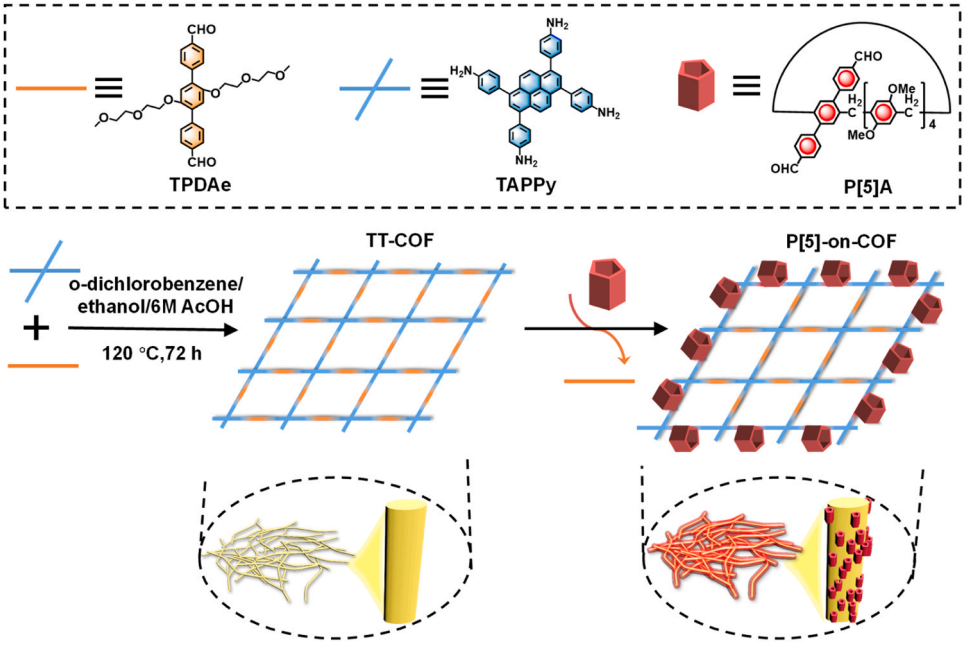

Scheme 1. Schematic illustration for the synthesis of hierarchical core-shell macrocycle-on-COF by in-situ linker exchange.

was characterized by ^{1}H NMR and Fourier-transform infrared (FT-IR) spectroscopy. Subsequently, the parent TT-COF was synthesized through a Schiff-base condensation reaction of TPDAe with TAPPy under solvothermal conditions with a mixed solvent of ethanol/o-dichlorobenzene/AcOH at 120 °C for 72 h (Scheme S4). Then, P[5]-on-COF was synthesized using TT-COF as cores and P[5]A as a new linker with partial linker exchange strategy by introducing 3 equivalents of P[5]A into suspensions of premade TT-COF in a mixed solvent of ethanol/AcOH at 120 °C for 72 h (Scheme S5).

Next, to demonstrate the successful COF-to-COF transformation, a series of chemical and microstructural characterization of TT-COF and P[5]-on-COF were conducted. As presented in the FT-IR spectra (Fig. 1a, Table S1), both the near-disappearance of aniline N-H stretching bands of TAPPy at 3361 cm^{-1} and the aldehydic carbonyl C═O bond of TPDAe at 1696 cm^{-1} in the spectrum of TT-COF indicate the consumption of the reactive groups. And a characteristic peak at 1624 cm^{-1} that attributed to C═N stretching vibration is observed, confirming the formation of C═N bond. The formed imine bonds have good reversibility, providing the possibility for subsequent linker exchange. Apparently, the profiles of the stretching bands of –CH_3 and –CH_2– (about 2950 cm^{-1}~2867 cm^{-1}) in the building blocks are different, probably due to the differences in the ratios of methyls and methylenes in TPDAe and P[5]A. Such characteristics also remain in the spectra of TT-COF and P[5]A-on-COF. In conformity with the results above, the C-O-C peak of TPDAe (1106 cm^{-1}) can be found in both the spectra of TT-COF and P[5]A-on-COF, while the C-O-C peak of P[5]A (1045 cm^{-1}) only appears in P[5]A-on-COF, demonstrating the successful realization of partial linker exchange. And the imine bonds are well maintained after linker exchange. Besides, to confirm the presence of both the original TPDAe and exchanged P[5]A linkers in P[5]-on-COF, hydrolysis experiment was performed. Concentrated HCl was used to hydrolyze the P[5]-on-COF powder, which was subsequently analyzed by ^{1}H NMR spectroscopy. The resulting spectrum (Fig. 1b) revealed simultaneous proton peaks belonging to the TPDAe (10.14 ppm) and P[5]A (10.11 ppm) aldehyde groups, indicating the successful occurrence of the linker exchange reaction. What's more, the ^{1}H NMR spectroscopy also revealed the extent of the linker exchange reaction, the integration areas of the peaks were found to be 37.97 and 32.38, corresponding to a degree of linker exchange up to ~ 54%.

The crystallinity of the as-formed TT-COF and P[5]-on-COF were checked with powder X-ray diffraction (PXRD). The comparisons between the PXRD patterns of the P[5]-on-COF and TT-COF show high

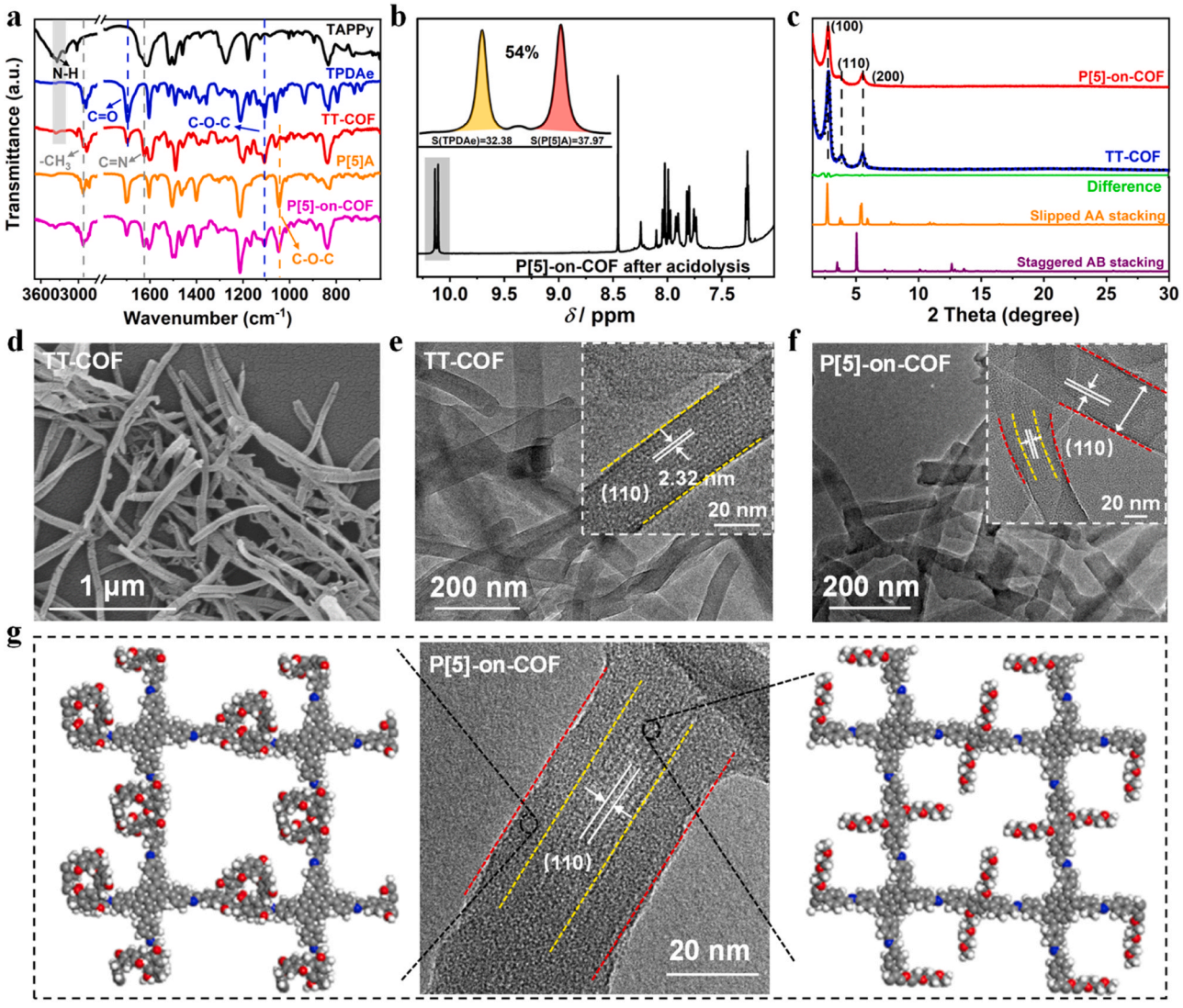

Fig. 1. (a) FT-IR spectra of building blocks, TT-COF and P[5]-on-COF. (b) ^{1}H NMR spectra of P[5]-on-COF after being treated with concentrated HCl in DMSO-d_6. (c) PXRD profiles of P[5]-on-COF (red) and TT-COF (blue), as well as Pawley refinement (black dashed line) of TT-COF and their difference (green), simulated by using AA-stacking (orange) models and AB-stacking (purple) models. (d) SEM images of TT-COF. (e-f) TEM images of TT-COF, P[5]-on-COF and the corresponding HR-TEM images (inset). (g) HR-TEM image and structure models of P[5]-on-COF clearly show the core-shell structure.

similarity (Fig. 1c), in which the diffraction peak at 2.71°, 3.82° and 5.50° were reasonably assigned to the (100), (110) and (220) diffractions, indicating that they have very similar lattice cells. The calculated diffraction patterns of TT-COF (Fig. 1c, Fig. S2, Tables S5-S6) based on the AA stacking model could reproduce the experimental data well, while the simulated profile of AB stacking mode showcased a huge difference. Furthermore, Pawley refinement was performed to optimize the unit cell parameters of TT-COF (a = 33.01 Å, b = 33.01 Å, c = 4.03 Å, $\alpha = \beta = 90°$, $\gamma = 92.59°$). Eventually, the final R_{WP} and R_P values converged to 7.74% and 6.16% for TT-COF, which resulted in satisfactorily low residual values and acceptable profile differences.

The microscopic morphologies were monitored by scanning electron microscopy (SEM) and transmission electron microscopy (TEM), which directly visualize the success of COF-to-COF transformation and the formation of core-shell architectures of P[5]-on-COF. As shown in Fig. 1d&e, the TT-COF shows nanometer fibrillar morphology, and the HR-TEM image reveals ordered lattice fringes throughout the nanofiber of the TT-COF from the inside to the outside. The lattice spacing of the regularly arranged lattice stripes is 2.32 nm, which corresponds well to the (110) crystal face of the TT-COF. After COF-to-COF transformation, the SEM image shows that the microscopic morphologies of P[5]-on-COF have little change (Fig. S3). However, the HR-TEM images show different characteristics. As shown in Fig. 1f, in some P[5]-on-COF fibers, the ordered lattice stripes appear only on the inner diameter of the nanofibers, while the edges are less pronounced. While in other fibers (Fig. 1f), the ordered lattice fringes spread the whole nanofibers. We attribute the outer part with less pronounced lattice stripes to the newly formed COF with rich P[5] units, while the inner part to the parent TT-COF. The bulky P[5] units lead to weak interlayer interaction, making it easier to lose its long-range order under electron irradiation. The yellow dashed lines in Fig. 1f&g highlight the core of the parent COF while the yellow and red dashed lines highlight the newly formed COF, the corresponding structural models are shown in Fig. 1g, which directly indicates the formation of core-shell architectures of P[5]-on-COF. The direct imaging of the core-shell architectures clearly shows the process of COF-to-COF transformation happens in a heterogeneous way occurring at the solid-solution interface. Based on the above experimental results and previous reports [23,24], a transformation mechanism has been proposed, and shown in Scheme S6.

Next, varying amounts of P[5]A (1, 3, 6, 10 eq.) were used in linker exchange reactions to elucidate the its effect on COF-to-COF transformation. PXRD (Fig. S4) demonstrated that all macrocycle-on-COFs generated from the partial linker exchange reaction preserved the crystallinity of TT-COF to a certain extent. The impact of P[5]A amounts on the extent of the exchange was analyzed via acid hydrolysis experiments. The exchange degree of the P[5]A linker was determined by evaluating the ratio of aldehyde peak areas, with results of ~ 44%, ~ 54%, ~ 58%, and ~ 70%, respectively (Fig. S5). The results indicate a

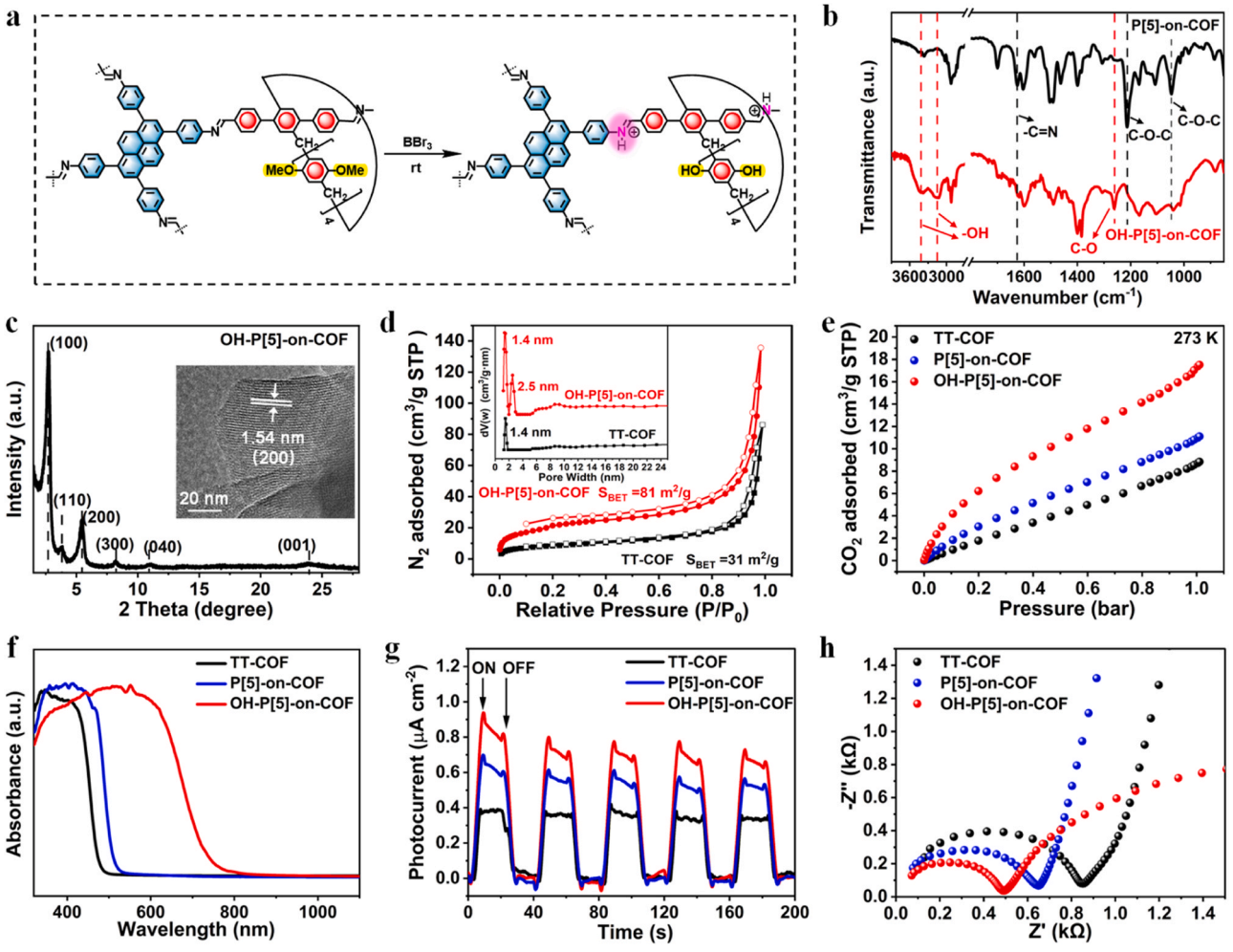

Fig. 2. (a) Schematic illustration for the synthesis of OH-P[5]-on-COF. (b) FT-IR spectra of P[5]-on-COF and OH-P[5]-on-COF. (c) PXRD pattern and HR-TEM image (inset) of OH-P[5]-on-COF. (d) N_2 adsorption-desorption isotherms and NLDFT pore size distributions (inset) of TT-COF and OH-P[5]-on-COF at 77 K. (e) The adsorption isotherms of CO_2 of TT-COF, P[5]-on-COF and OH-P[5]-on-COF at 273 K, respectively. (f-h) UV/vis absorption spectra, transient photocurrent responses, electrochemical impedance spectroscopy (EIS) Nyquist plots of TT-COF (black), P[5]-on-COF (blue) and OH-P[5]-on-COF (red), respectively.

rising trend in the degree of linker exchange with an increased amount of P[5]A involved in the linker exchange reaction.

3.2. Functionalization of P[5]-on-COF

In order to improve the ability of CO_2 adsorption and introduce active sites, we further functionalized the P[5]-on-COF to obtain hydroxylated OH-P[5]-on-COF that with hydrogen-bond donors. As shown in Fig. 2a, the OH-P[5]-on-COF was synthesized by BBr_3 demethylation of P[5]-on-COF at room temperature condition [24]. The FT-IR of OH-P[5]-on-COF demonstrated that the characteristic peaks of C-O-C (1211 cm^{-1} and 1047 cm^{-1}) [35] of anisole were nearly eliminated, whereas the -OH vibration peaks appeared at 3148 cm^{-1} and 3418 cm^{-1}, and a new characteristic peak of C-O emerged at 1263 cm^{-1}, which confirms the successful formation of OH-P[5]-on-COF (Fig. 2b). The hydrolysis experiment of OH-P[5]-on-COF demonstrates that all the methoxy groups were converted to hydroxyl groups after the demethylation reaction. (Fig. S6). The SEM images showed that OH-P[5]-on-COF kept nanofibrous morphology (Fig. S7) and the PXRD demonstrated that OH-P[5]-on-COF possessed high crystallinity, the diffraction peak at 2.70°, 3.79°, 5.47°, 8.20°, 10.92°, and 23.95° were attributed to (100), (110), (200), (300), (040), and (001) crystal planes, respectively (Fig. 2c). Furthermore, the HR-TEM images of OH-P[5]-on-COF (Fig. 2c, inset) showed distinct lattice fringes. On the whole, the microscopic morphologies and crystallinity of OH-P[5]-on-COF show high similarity with TT-COF and P[5]-on-COF.

3.3. Structure characterization and photoelectrical properties of OH-P[5]-on-COF

The porosity of TT-COF, P[5]-on-COF and OH-P[5]-on-COF was evaluated by nitrogen adsorption-desorption measurement (Fig. 2d and Fig. S8). Derived from the data of sorption isotherm in the low-pressure region ($0.1 < P/P_0 < 0.2$), the Brunauer-Emmett-Teller (BET) surface areas of TT-COF, P[5]-on-COF and OH-P[5]-on-COF were calculated to be 31, 53 and 81 $m^2\ g^{-1}$, and the corresponding total pore volume (at $P/P_0 = 0.98$) were 0.13, 0.13 and 0.21 $cm^3\ g^{-1}$ respectively. The pore size distribution (PSD) was analyzed using nonlocal density functional theory (NLDFT). Two main distribution peaks of OH-P[5]-on-COF were observed at 1.4 and 2.5 nm (Fig. 2d, inset), belonging to the pore sizes of the parental TT-COF and the newly formed OH-P[5]-on-COF respectively [36], which indicated that OH-P[5]-on-COF possesses hierarchical pore structure.

In the catalytic conversion of CO_2, the density of binding sites and their binding strength with CO_2 in catalysts are vital to their performance. Therefore, the CO_2 adsorption capacity of the OH-P[5]-on-COF was investigated by CO_2 physical adsorption (Fig. 2e). P[5]-on-COF (11.107 cm^3/g) containing pillararene groups exhibited much higher CO_2 adsorption capacity than TT-COF (8.839 cm^3/g). It suggests that the introduction of pillararene in COFs can enhance their adsorption capacity for CO_2. What's more, OH-P[5]-on-COF exhibited an even greater CO_2 adsorption capacity of 17.51 cm^3/g, which is attributed to the dipole interactions between CO_2 and the hydroxyl groups of OH-P[5]-on-COF [24,25,37]. These strong interactions are expected to bring about extraordinary CO_2 activation ability.

The broad range light absorption and efficient charge separation play a crucial role in achieving an efficient photocatalytic CO_2 cycloaddition reaction. Accordingly, the photoelectric properties of OH-P[5]-on-COF were investigated in detail. As shown in Fig. 2f, diffuse reflectance ultraviolet-visible (UV–vis) spectra show distinct changes between the COFs. TT-COF exhibits an absorbance edge around 520 nm, whereas the absorbance edge is red-shifted to 570 and 890 nm for P[5]-on-COF and OH-P[5]-on-COF, respectively. Additional investigation into the wider range of light absorption properties displayed by OH-P[5]-on-COF revealed that it can be attributed to the protonation of imine bonds and the introduction of hydroxyl groups (for detailed information, see the Supporting Information, Fig. S9-S10). Transient photocurrent measurements and electrochemical impedance spectroscopy (EIS) were conducted to further explore the exciton separation and the charge transfer [38,39]. The visible light on/off transient photocurrent curves of TT-COF, P[5]-on-COF, and OH-P[5]-on-COF were obtained under chopped illumination to explore the charge migration process being responsible for the photocatalytic reaction. In Fig. 2g, compared to TT-COF (0.40 $\mu A \cdot cm^{-2}$) and P[5]-on-COF (0.62 $\mu A \cdot cm^{-2}$), the photocurrent density of OH-P[5]-on-COF exhibits a significant increase (0.80 $\mu A \cdot cm^{-2}$), which manifests the fast photoresponse and the significantly boosted separation and transfer of photoinduced charge carriers of OH-P[5]-on-COF. The much smaller semicircular diameter of OH-P[5]-on-COF electrode in the EIS Nyquist plot (Fig. 2h) indicates lower electrical resistance and faster interfacial charge transfer than those of TT-COF and P[5]-on-COF. Based on the above illustration of the photoelectric properties, OH-P[5]-on-COF is expected to have great potential for photocatalytic reactions.

3.4. Photocatalytic CO_2 cycloaddition

Combining the unique structural features and excellent photoelectrical properties, OH-P[5]-on-COF is expected to achieve high photocatalytic efficiency in CO_2 cycloaddition reaction under ambient conditions (Fig. 3a). As can be seen from Fig. 3b, a 99% conversion of epichlorohydrin can be achieved within 3 h under light irradiation over OH-P[5]-on-COF. It is noteworthy that the reaction condition is mild (20 °C and 1 atm), and the performance is superior compared to previously reported COFs (Fig. 3c, Table S2). Control experiments were further carried out to check the influencing factors of this reaction in detail (Fig. 3b and Table S3). Obviously, without the co-catalyst TBAB, the conversion reduces to a negligible level. Therefore, the TBAB plays a crucial role in the CO_2 cycloaddition reaction. The TBAB was used as a nucleophilic co-catalyst, in which the Br^- attack the least hindered β-carbon atom of the epoxide, leading to the opening of the epoxide ring and facilitating reaction progression [40,41].

However, only in the presence of TBAB, the conversion is very low (11%), exhibiting the significant role of catalyst in improving the efficiency. Furthermore, the conversion reduces to 14% in the dark even in the presence of TBAB and OH-P[5]-on-COF, suggesting that light is essential for this reaction when OH-P[5]-on-COF is used as the catalyst. FT-IR, XRD and HR-TEM characterization after the photocatalytic test confirmed the stability of OH-P[5]-on-COF (Fig. S12-S14). The catalytic activity of OH-P[5]-on-COF remained as much as nearly 95% of the initial value after additional three recycling tests (Fig. S15), suggesting adequate recyclability and stability for CO_2 cycloaddition reaction.

Encouraged by the excellent catalytic activity of OH-P[5]-on-COF towards the CO_2 cycloaddition with epichlorohydrin, various epoxides with different substituents have also been investigated. As summarized in Fig. 3d, Table S4 and Fig. S16-S21, the conversions of CO_2 with epichlorohydrin, 1,2-epoxybutane, and 1,2-epoxyhexane all reached 99%. Similarly, the reaction conversions with 2,3-epoxy-1-propanol and 4-bromo-1,2-epoxy-butane were 93% and 95%, respectively. However, the conversion was only 67% when styrene oxide was chosen as the reaction substrate. The reduced conversion can be reasonably explained by the steric hindrance effect of their large substituent [22,42]. The above results indicate that OH-P[5]-on-COF exhibits admirable substrate universality in the highly efficient photocatalytic CO_2 cycloaddition under ambient conditions.

3.5. Investigation of mechanism

To explore the structure-property correlation in the photocatalytic system, corresponding comparative tests were carried out on OH-MCR-54%, P[5]-on-COF and TT-COF under the same conditions. The OH-MCR-54% was synthesized by multicomponent reaction (molar ratio, TAPPy: TPDAe: P[5]A = 0.020: 0.018: 0.022), and the active sites were

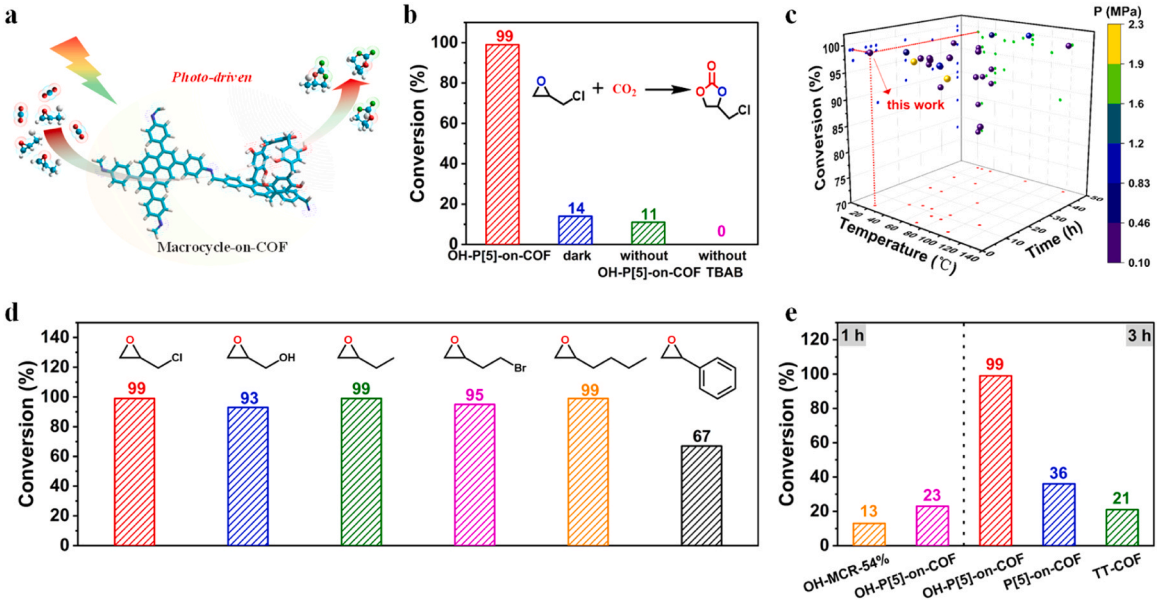

Fig. 3. (a) Schematic illustration of the photocatalytic CO_2 cycloaddition over OH-P[5]-on-COF. (b) The conversions for CO_2 cycloaddition reaction within 3 hours under different conditions. (c) Comparison of catalytic activity of COF-based catalysts for CO_2 cycloaddition. (d) Synthesis of various cyclic carbonates catalyzed by OH-P[5]-on-COF. Reaction conditions: epoxide (0.25 mmol), catalyst (1.5 g), co-catalyst TBAB (0.0125 mmol), CO_2 (1 atm), temperature (T = 20°C), reaction time (epichlorohydrin: 3 h, while for the others is 8 h.). (e) Catalytic performance comparison for CO_2 cycloaddition reaction with different catalysts.

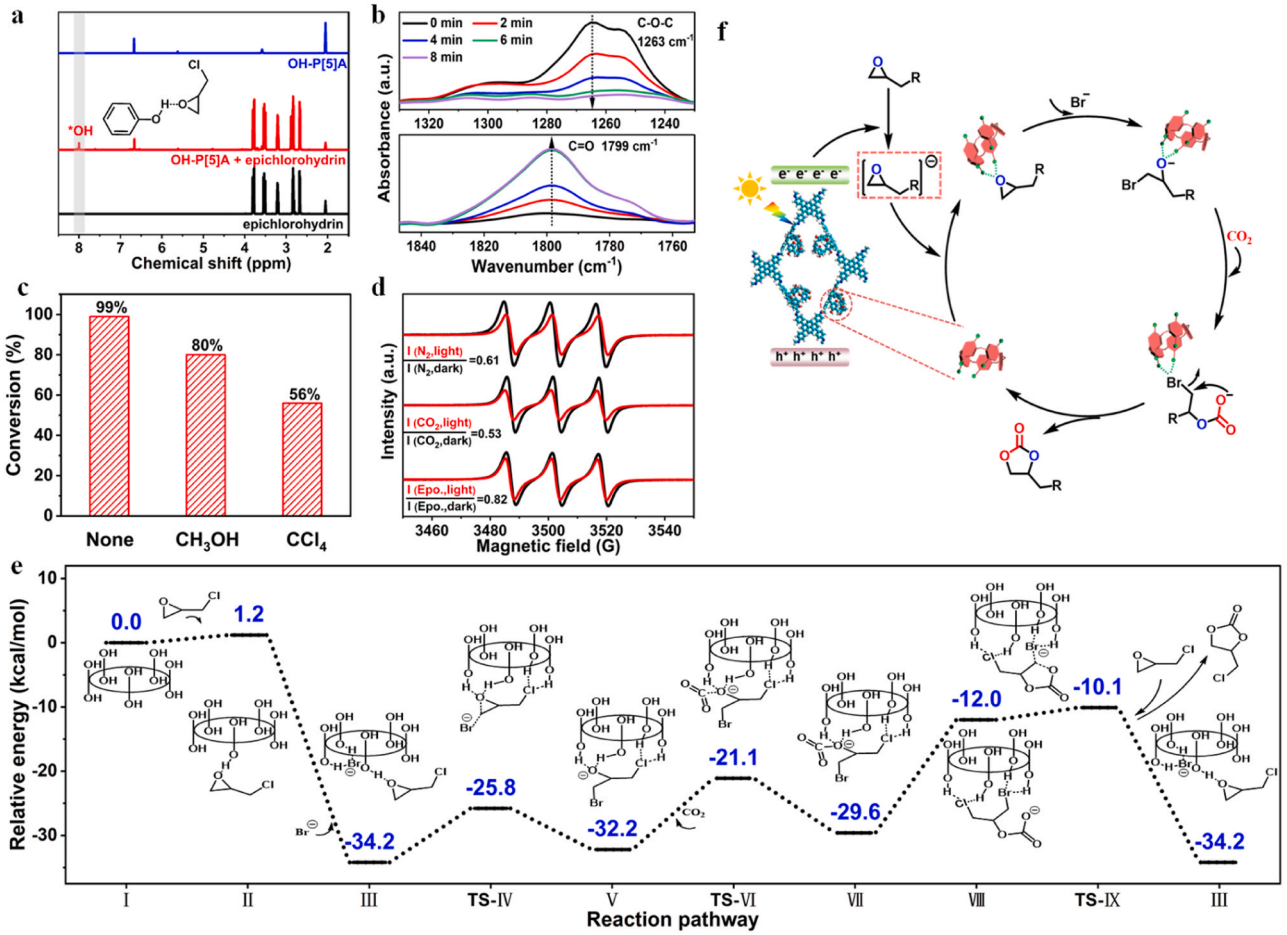

Fig. 4. (a) ^1H NMR spectra of OH-P[5]A, epichlorohydrin, and a mixture of OH-P[5]A and epichlorohydrin. (b) The *in situ* FT-IR spectrum for detecting photocatalytic CO_2 cycloaddition reaction over OH-P[5]-on-COF. (c) Quenching experiments with different sacrificial agents using OH-P[5]-on-COF as a catalyst. (d) EPR spectra of OH-P[5]-on-COF under N_2 atmosphere, CO_2 atmosphere, and with epichlorohydrin in N_2 atmosphere. (e) Potential energy profiles of CO_2 cycloaddition reaction with epichlorohydrin on OH-P[5]A. (f) Proposed mechanism of photo-driven CO_2 cycloaddition reaction over OH-P[5]-on-COF.

supposed to randomly scattered over the catalysts (for detailed information, see the Supporting Information, Fig. S22). As shown in Fig. 3e, the OH-MCR-54% showed a lower conversion (13% for 1 hour, 89% for 3 hours, Table S3) than OH-P[5]-on-COF (23% for 1 hour, 99% for 3 hours, Table S3), which indicates that core-shell structure of OH-P[5]-on-COF could more fully expose the active sites and gain higher catalytic efficiency. In addition, control experiments were conducted to examine the influence of the exchange degree of P[5]A linker (Figure S23) and protonated imine bonds (Figure S24) on the photocatalytic performance toward the CO_2 cycloaddition reaction, respectively.

Next, the role of the hydroxyls was studied. Without the hydroxyls, P[5]-on-COF and TT-COF exhibited low efficiencies of CO_2 cycloaddition reaction (about 36% and 21% respectively, Fig. 3e), indicating the hydroxyls of OH-P[5]-on-COF is a key factor for the CO_2 cycloaddition reaction. Past research has shown that hydrogen bond donors (e.g., hydroxyl and carboxyl groups) can activate epoxides through hydrogen bonding, facilitating the ring opening and subsequent CO_2 insertion [43]. Herein, the ^{1}H NMR analyses were performed to understand the interaction of micromolecular perhydroxyl-pillar[5]arene (OH-P[5]A) with epichlorohydrin. As shown in Fig. 4a, no signal of the phenolic hydroxyl group was observed in the spectrum of OH-P[5]A, however, the signal at ~8 ppm was found in the ^{1}H NMR spectra of OH-P[5]A and epichlorohydrin mixture. This phenomenon can be reasonably explained as that the H of hydroxyl group in OH-P[5]A is too active to detect at room temperature, but when epichlorohydrin was added, the generated H-bond "fixed" the H of the -OH, leading to the emergence of the signal of H. The H-bond formation between OH-P[5]-on-COF and epoxides can activate epoxides and facilitate the ring opening.

In addition, *in situ* FT-IR spectra were conducted to track the reaction process of the cycloaddition of CO_2 and epichlorohydrin (Fig. 4b). The characteristic absorption peak (C═O stretching vibration) of cyclic carbonate at 1799 cm^{-1} emerged and gradually intensified [44]. Meanwhile, the consumption of epichlorohydrin was also confirmed by the disappearance of the peak at 1263 cm^{-1}, which was assigned to the ring vibration of C-O-C epoxy group [45]. The above results proved that the cycloaddition reaction of epoxides and CO_2 proceeded efficiently.

The control experiments showed that light is essential for the reaction when OH-P[5]-on-COF was used as the catalyst, the conversion is only 14% in the dark (Fig. 3b). Thus, the mechanism of the photocatalytic CO_2 cycloaddition reaction were studied in more detail. First, the role of photo-generated electrons and holes in the reaction was verified through capture experiments. Trapping experiments of e^- and h^+ were conducted by adding carbon tetrachloride (CCl_4) and methanol (CH_3OH), respectively. As shown in Fig. 4c, when CH_3OH was added, the conversion of epichlorohydrin reduced from 99% to 80%, whereas the conversion observably decreased with the addition of CCl_4 (from 99% to 54%), suggesting that the electrons were the major active species involved in the photocatalytic CO_2 cycloaddition reaction. To further examine the transfer path of the photo-generated electrons, as shown in Fig. 4d, the electron paramagnetic resonance (EPR) measurements were performed at different conditions [46,47]. 2,2,6,6-Tetramethylpiperidine-1-oxyl (TEMPO) is used as the EPR spin label. In N_2 atmosphere, the spectral intensities (I) significantly reduced after irradiation, and the calculated I (N_2, light)/I (N_2, dark) is 0.61. This decrease is attributed to that electrons generated in OH-P[5]-on-COF under illumination are captured by TEMPO, and partial TEMPO form the negative ion species $TEMPO^-$. $TEMPO^-$ has no unpaired electrons and is EPR silent. A similar intensity reduction is observed when the EPR test is performed in CO_2 atmosphere, with an I (CO_2, light)/I (CO_2, dark) of 0.53. This confirms that the photo-generated electrons can't transfer to CO_2, but are captured by TEMPO. In contrast, the intensity of the triplet peak has a minor change (I (epo., light)/I (epo., dark) is 0.82) after illumination when epichlorohydrin was added. This result indicates that the photo-generated electrons were transferred to the epoxides and thus TEMPO can still maintain the content of unpaired electrons. According to the above analysis, the photo-generated electrons transfer to epoxides instead of CO_2 during the photocatalytic reaction. The early finding suggests that electrons transfer to epoxides forming a negatively charged intermediate, which has enough energy to supplement the energy-cost in ring-opening step, and thus no additional energy is required in the photo-driven catalysis process [48].

In order to gain a deeper insight into the role of hydroxyl groups, we performed the DFT calculations to investigate the OH-P[5]A-catalyzed CO_2 cycloaddition process. Fig. 4e presents the calculated Gibbs free energy curves for the cycloaddition of epoxide and CO_2 catalyzed by micromolecular perhydroxyl-pillar[5]arene (OH-P[5]A) in the presence of TBAB along with the structure of intermediates and transition states. Firstly, OH-P[5]A interacted with epoxide via hydrogen bond is slightly endergonic and leads to intermediate **II** that lies 1.2 kcal/mol above OH-P[5]A. Next, the opening of the epoxide ring leads to the formation of intermediate **V** with a lower energy (-32.2 kcal/mol). Afterward, the electrophilic attack of CO_2 on the O of intermediate **V** leads to another intermediate (**VII**), which lies −29.6 kcal/mol below OH-P[5]A. The CO_2 insertion step requires overcoming of a barrier (**TS-VI**) of 11.1 kcal/mol relative to intermediate **V**. Subsequently, the negative charges transfer from the O of epichlorohydrin to the O of CO_2, forming the intermediate **VIII**. This step possesses an energy barrier of 17.6 kcal/mol, making it the rate-limiting step throughout the whole reaction path. The last step is intermolecular ring closure to produce the desired cyclic carbonate, with an energy barrier of 1.9 kcal/mol (**TS-IX**) relative to intermediate **VIII**. The regeneration of intermediates **III**, which participates in the next catalytic cycle, is accompanied by the ring closure step.

In previous reports, it has also been demonstrated that the ring-opening step of adsorbed epoxides is the rate-limiting step [46,48,49]. However, in our case, upon the entry of Br^- into the system, the dense electron cloud is initially bound by two hydrogen bonds concurrently, reducing the energy to −34.2 kcal/mol. The multiple hydrogen bond effect provides support for the stable system energy to promote the occurrence of the reaction path under low energy conditions. Subsequently, Cl^- replaces the Br^- bound by hydrogen bonds, and Br^- realizes nucleophilic attack by overcoming an energy barrier of 8.4 kcal/mol. This is attributed to the existence of multi-hydroxyl groups which have H-bonding with the O of epichlorohydrin, endowing the activation of epichlorohydrin and enhancing the reactivity of CO_2 cycloaddition. And thus enable the reaction to proceed under ambient conditions. Overall, these computational results show the key role of the OH groups in OH-P[5]-on-COF. They can not only assist the ring-opening of epoxides but also stabilize intermediates and transition states by means of inter- and intramolecular hydrogen bonds.

Based on the results above and the previous reports [48,50], a plausible mechanism for the photocatalytic CO_2 cycloaddition reaction using OH-P[5]-on-COF as a photo-catalyst has been proposed in Fig. 4 f. Initially, the photo-generated electrons are favorably transferred from the OH-P[5]-on-COF to the epoxides and make them negatively charged. The oxygen atom of the epoxides interacts with hydroxyl groups of OH-P[5]-on-COF to form multiple intermolecular hydrogen bonds, resulting in the activation of the epoxides. Simultaneously, the bromide anion in TBAB as Lewis base nucleophilicly attacked on the less sterically hindered β-carbon atom of epoxides, facilitating the ring-opening of epoxides. Next, the carbon atom of CO_2 is attacked by the oxygen anion in the ring-opened intermediate and thus CO_2 is inserted into the intermediate, resulting in the formation of a bromocarbonate complex. Finally, the ring undergoes subsequent intramolecular closure, resulting in the formation of a cyclic carbonate and the regeneration of the catalyst. Hence, the synergistic activation of the photo-generated exciton, the multiple-hydrogen-bond effect and the bromide ion as a nucleophile, facilitate the cycloaddition reaction smoothly under ambient conditions.

4. Conclusion

In summary, a "Macrocycle-on-COF" strategy was presented here to

coordinatively functionalize COFs with pillar[5]arene by partial in-situ linker exchange to gain core-shell hybrids, while retaining the crystallinity of the parent framework. The resulting OH-P[5]-on-COF exhibited improved CO_2 adsorption capacity and excellent photoelectric properties. More importantly, the OH-P[5]-on-COF can serve as efficient heterogeneous catalysts that realize highly efficient photocatalytic CO_2 cycloaddition reaction under ambient conditions (20 °C and 1 atm), which show superior performance compared to previously reported COFs. This study presents the first example of using COFs as photocatalysts for photocatalytic CO_2 cycloaddition reaction under ambient conditions. These findings pave the way to the development of advanced COFs materials with enhanced properties by simply integrating existing macrocycle onto diverse parent COFs from the database.

CRediT authorship contribution statement

Xiaojuan Li: Writing – original draft, Investigation, Data curation, Conceptualization. **Xinxin Niu:** Writing – original draft, Investigation, Data curation. **Peng Fu:** Investigation. **Wenping Hu:** Resources, Project administration, Funding acquisition. **Guangyuan Feng:** Writing – review & editing, Writing – original draft, Project administration, Funding acquisition, Data curation, Conceptualization. **Shengbin Lei:** Writing – review & editing, Supervision, Project administration, Funding acquisition, Conceptualization. **Yaru Song:** Investigation, Data curation. **Enbing Zhang:** Methodology, Data curation. **Yanfeng Dang:** Supervision, Project administration, Formal analysis, Data curation. **Jing Yan:** Writing – review & editing, Supervision, Methodology, Data curation.

Declaration of Competing Interest

The authors declare no competing interests.

Data Availability

Data will be made available on request.

Acknowledgments

This work was financially supported by the National Science Foundation of China (52073208), the China Postdoctoral Science Foundation (2022M722356), Seed Foundation of Tianjin University (2023XQM-0028, 2023XSU-0020) and the Fundamental Research Funds for the Central Universities.

Author contributions

G.F. conceived and directed the research. S.L. gave detailed guidance and funding acquisition X. L. performed the experiments and analyzed the data. X. N. and Y. D. gave assistance to perform DFT calculation. P. F. gave assistance to perform ^{1}H NMR investigation. Y. S., E. Z. and J. Y. helped to analyze the data. W. H. provided guidance.

Appendix A. Supporting information

Supplementary data associated with this article can be found in the online version at doi:10.1016/j.apcatb.2024.123943.

References

[1] H. Chen, H.S. Jena, X. Feng, K. Leus, P. Van Der Voort, Engineering covalent organic frameworks as heterogeneous photocatalysts for organic transformations, Angew. Chem. Int. Ed. 61 (2022) e202204938, https://doi.org/10.1002/anie.202204938.
[2] Y. Gong, X. Guan, H. Jiang, Covalent organic frameworks for photocatalysis: synthesis, structural features, fundamentals and performance, Coord. Chem. Rev. 475 (2023) 214889, https://doi.org/10.1016/j.ccr.2022.214889.
[3] T. He, Y. Zhao, Covalent organic frameworks for energy conversion in photocatalysis, Angew. Chem. Int. Ed. 62 (2023) e202303086, https://doi.org/10.1002/anie.202303086.
[4] S. Liu, M. Wang, Y. He, Q. Cheng, T. Qian, C. Yan, Covalent organic frameworks towards photocatalytic applications: Design principles, achievements, and opportunities, Coord. Chem. Rev. 475 (2023) 214882, https://doi.org/10.1016/j.ccr.2022.214882.
[5] A. López-Magano, S. Daliran, A.R. Oveisi, R. Mas-Ballesté, A. Dhakshinamoorthy, J. Alemán, H. Garcia, R. Luque, Recent advances in the use of covalent organic frameworks as heterogenous photocatalysts in organic synthesis, Adv. Mater.. 35 (2023) 2209475, https://doi.org/10.1002/adma.202209475.
[6] M.-Y. Zhang, J.-K. Li, R. Wang, S.-N. Zhao, S.-Q. Zang, T.C.W. Mak, Construction of core–shell MOF@COF hybrids with controllable morphology adjustment of COF shell as a novel platform for photocatalytic cascade reactions, Adv. Sci. 8 (2021) 2101884, https://doi.org/10.1002/advs.202101884.
[7] G. Li, S. Dong, P. Fu, Q. Yue, Y. Zhou, J. Wang, Synthesis of porous poly(ionic liquid)s for chemical CO_2 fixation with epoxides, Green. Chem. 24 (2022) 3433–3460, https://doi.org/10.1039/D2GC00324D.
[8] R. Luo, M. Chen, F. Zhou, J. Zhan, Q. Deng, Y. Yu, Y. Zhang, W. Xu, Y. Fang, Synthesis of metalloporphyrin-based porous organic polymers and their functionalization for conversion of CO_2 into cyclic carbonates: recent advances, opportunities and challenges, J. Mater. Chem. A 9 (2021) 25731–25749, https://doi.org/10.1039/D1TA08146B.
[9] Q.-J. Wu, J. Liang, Y.-B. Huang, R. Cao, Thermo-, Electro-, and Photocatalytic CO_2 Conversion to value-added products over porous metal/covalent organic frameworks, Acc. Chem. Res. 55 (2022) 2978–2997, https://doi.org/10.1021/acs.accounts.2c00326.
[10] G. Cai, P. Yan, L. Zhang, H.-C. Zhou, H.-L. Jiang, Metal–organic framework-based hierarchically porous materials: synthesis and applications, Chem. Rev. 121 (2021) 12278–12326, https://doi.org/10.1021/acs.chemrev.1c00243.
[11] Z. Mu, Y. Zhu, Y. Zhang, A. Dong, C. Xing, Z. Niu, B. Wang, X. Feng, Hierarchical microtubular covalent organic frameworks achieved by COF-to-COF transformation, Angew. Chem. Int. Ed. 62 (2023) e202300373, https://doi.org/10.1002/anie.202300373.
[12] Q. Sun, Z. Dai, X. Meng, F.-S. Xiao, Porous polymer catalysts with hierarchical structures, Chem. Soc. Rev. 44 (2015) 6018–6034, https://doi.org/10.1039/C5CS00198F.
[13] X.-Y. Yang, L.-H. Chen, Y. Li, J.C. Rooke, C. Sanchezc, B.-L. Su, Hierarchically porous materials: synthesis strategies and structure design, Chem. Soc. Rev. 46 (2017) 481–558, https://doi.org/10.1039/C6CS00829A.
[14] G. Zhang, M. Tsujimoto, D. Packwood, N.T. Duong, Y. Nishiyama, K. Kadota, S. Kitagawa, S. Horike, Construction of a hierarchical architecture of covalent organic frameworks via a postsynthetic approach, J. Am. Chem. Soc. 140 (2018) 2602–2609, https://doi.org/10.1021/jacs.7b12350.
[15] W. Li, J. Wang, J. Chen, K. Chen, Z. Wen, A. Huang, Core–shell carbon-based bifunctional electrocatalysts derived from COF@MOF hybrid for advanced rechargeable Zn–air batteries, Small 18 (2022) 2202018, https://doi.org/10.1002/smll.202202018.
[16] B.J. Smith, W.R. Dichtel, Mechanistic studies of two-dimensional covalent organic frameworks rapidly polymerized from initially homogenous conditions, J. Am. Chem. Soc. 136 (2014) 8783–8789, https://doi.org/10.1021/ja5037868.
[17] B.J. Smith, A.C. Overholts, N. Hwang, W.R. Dichtel, Insight into the crystallization of amorphous imine-linked polymer networks to 2D covalent organic frameworks, Chem. Commun. 52 (2016) 3690–3693, https://doi.org/10.1039/C5CC10221A.
[18] S. Wang, Y. Yang, P. Liu, Z. Zhang, C. Zhang, A. Chen, O.O. Ajao, B.-G. Li, P. Braunstein, W.-J. Wang, Core-shell and yolk-shell covalent organic framework nanostructures with SIze-selective Permeability, Cell Rep. Phys. Sci. 1 (2020) 100062, https://doi.org/10.1016/j.xcrp.2020.100062.
[19] R. Luo, Y. Yang, K. Chen, X. Liu, M. Chen, W. Xu, B. Liu, H. Ji, Y. Fang, Tailored covalent organic frameworks for simultaneously capturing and converting CO_2 into cyclic carbonates, J. Mater. Chem. A 9 (2021) 20941–20956, https://doi.org/10.1039/D1TA05428G.
[20] M. Yin, L. Wang, S. Tang, Stable dicationic covalent organic frameworks manifesting notable structure-enhanced CO_2 capture and conversion, ACS Catal. 13 (2023) 13021–13033, https://doi.org/10.1021/acscatal.3c02796.
[21] D. Ma, Y. Song, H. Zhao, C. Yu, Y. Zhang, C. Li, K. Liu, Ordered macro–microporous covalent organic frameworks as bifunctional catalysts for CO_2 cycloaddition, ACS Sustain. Chem. Eng. 11 (2023) 6183–6190, https://doi.org/10.1021/acssuschemeng.2c06816.
[22] F. Yang, Y. Li, T. Zhang, Z. Zhao, G. Xing, L. Chen, Docking site modulation of isostructural covalent organic frameworks for CO_2 fixation, Chem. Eur. J. 26 (2020) 4510–4514, https://doi.org/10.1002/chem.202000552.
[23] D. Dai, J. Yang, Y.-C. Zou, J.-R. Wu, L.-L. Tan, Y. Wang, B. Li, T. Lu, B. Wang, Y.-W. Yang, Macrocyclic arenes-based conjugated macrocycle polymers for highly selective CO_2 capture and iodine adsorption, Angew. Chem. Int. Ed. 60 (2021) 8967–8975, https://doi.org/10.1002/anie.202015162.
[24] M.-M. Zhai, C.-Y. Wu, Y.A. Liu, W.-B. Hu, H. Yang, K. Wen, Hydroxy-Rich Pillar[5]arene-Based Nanoporous Aromatic Frameworks (PAFs) for Efficient CO_2 Uptake under Ambient Conditions, ACS Appl. Nano Mater. 5 (2022) 14221–14226, https://doi.org/10.1021/acsanm.2c03045.
[25] L.-L. Tan, H. Li, Y. Tao, S.X.-A. Zhang, B. Wang, Y.-W. Yang, Pillar[5]arene-Based Supramolecular Organic Frameworks for Highly Selective CO_2-Capture at Ambient Conditions, Adv. Mater. 26 (2014) 7027–7031.
[26] L. Liu, Z. Liu, J. Cui, G. Ning, W. Gong, Insertion of pillar[5]arene into Tröger's base-derived porous organic polymer for promoted heterogeneous catalytic

performance in Knoevenagel condensation and CO_2 fixation, Chin. Chem. Lett. 35 (2024) 108422, https://doi.org/10.1016/j.cclet.2023.108422.
[27] C. Qian, Q.-Y. Qi, G.-F. Jiang, F.-Z. Cui, Y. Tian, X. Zhao, Toward Covalent Organic Frameworks Bearing Three Different Kinds of Pores: The Strategy for Construction and COF-to-COF Transformation via Heterogeneous Linker Exchange, J. Am. Chem. Soc. 139 (2017) 6736–6743, https://doi.org/10.1021/jacs.7b02303.
[28] Z. Li, X. Ding, Y. Feng, W. Feng, B.-H. Han, Structural and Dimensional Transformations between Covalent Organic Frameworks via Linker Exchange, Macromolecules 52 (2019) 1257–1265, https://doi.org/10.1021/acs.macromol.8b01814.
[29] D.-L. Ma, Q.-Y. Qi, J. Lu, M.-H. Xiang, C. Jia, B.-Y. Lu, G.-F. Jiang, X. Zhao, Transformation between 2D covalent organic frameworks with distinct pore hierarchy via exchange of building blocks with different symmetries, Chem. Commun. 56 (2020) 15418–15421, https://doi.org/10.1039/D0CC06536F.
[30] Z.-B. Zhou, P.-J. Tian, J. Yao, Y. Lu, Q.-Y. Qi, X. Zhao, Toward azo-linked covalent organic frameworks by developing linkage chemistry via linker exchange, Nat. Commun. 13 (2022) 2180, https://doi.org/10.1038/s41467-022-29814-3.
[31] M.K. Shehab, K.S. Weeraratne, O.M. El-Kadri, V.K. Yadavalli, H.M. El-Kaderi, Templated Synthesis of 2D Polyimide Covalent Organic Framework for Rechargeable Sodium-Ion Batteries, Macromol. Rapid. Commun. 44 (2023) 2200782, https://doi.org/10.1002/marc.202200782.
[32] A.P. Côté, A.I. Benin, N.W. Ockwig, M. O'Keeffe, A.J. Matzger, O.M. Yaghi, Porous, Crystalline, Covalent Organic Frameworks, Science 310 (2005) 1166–1170, https://doi.org/10.1126/science.1120411.
[33] G. Feng, Q. Luo, M. Li, Y. Song, Y. Shen, S. Lei, W. Hu, Construction and nanotribological study of a glassy covalent organic network on surface, Nano Res 15 (2022) 4682–4686, https://doi.org/10.1007/s12274-021-3988-5.
[34] C. Fan, H. Wu, J. Guan, X. You, C. Yang, X. Wang, L. Cao, B. Shi, Q. Peng, Y. Kong, Y. Wu, N.A. Khan, Z. Jiang, Scalable Fabrication of Crystalline COF Membranes from Amorphous Polymeric Membranes, Angew. Chem. Int. Ed. 60 (2021) 18051–18058, https://doi.org/10.1002/anie.202102965.
[35] T. Ogoshi, T. Aoki, K. Kitajima, S. Fujinami, T.-a Yamagishi, Y. Nakamoto, Rapid, and High-Yield Synthesis of Pillar[5]arene from Commercially Available Reagents and Its X-ray Crystal Structure, J. Org. Chem. 76 (2011) 328–331, https://doi.org/10.1021/jo1020823.
[36] W. Ji, P. Zhang, G. Feng, Y.-Z. Cheng, T.-X. Wang, D. Yuan, R. Cha, X. Ding, S. Lei, B.-H. Han, Synthesis of a covalent organic framework with hetero-environmental pores and its medicine co-delivery application, Nat. Commun. 14 (2023) 6049, https://doi.org/10.1038/s41467-023-41622-x.
[37] L.-L. Tan, Y. Zhu, Y. Jin, W. Zhang, Y.-W. Yang, Highly CO_2 selective pillar[n]arene-based supramolecular organic frameworks, Supramol. Chem. 30 (2018) 648–654, https://doi.org/10.1080/10610278.2018.1427239.
[38] G. Feng, Y. Sun, J. Yuan, J. Qian, N. Siam, D. Fa, W. Ji, E. Zhang, Y. Shen, J. Yan, S. Lei, W. Hu, A CMP-based [FeFe]-hydrogenase dual-functional biomimetic system for photocatalytic hydrogen evolution coupled with degradation of tetracycline, Appl. Catal. B 340 (2024) 123200, https://doi.org/10.1016/j.apcatb.2023.123200.
[39] J.-P. Jeon, Y.J. Kim, S.H. Joo, H.-J. Noh, S.K. Kwak, J.-B. Baek, Benzotrithiophene-based Covalent Organic Framework Photocatalysts with Controlled Conjugation of Building Blocks for Charge Stabilization, Angew. Chem., Int. Ed. 62 (2023) e202217416, https://doi.org/10.1002/anie.202217416.
[40] N. Sharma, B. Ugale, S. Kumar, K. Kailasam, Metal-Free Heptazine-Based Porous Polymeric Network as Highly Efficient Catalyst for CO_2 Capture and Conversion, Front. Chem. 9 (2021) 737511, https://doi.org/10.3389/fchem.2021.737511.
[41] S. Ravi, P. Puthiaraj, W.-S. Ahn, Hydroxylamine-Anchored Covalent Aromatic Polymer for CO_2 Adsorption and Fixation into Cyclic Carbonates, ACS Sustain. Chem. Eng. 6 (2018) 9324–9332, https://doi.org/10.1021/acssuschemeng.8b01588.
[42] Y. Li, X. Song, G. Zhang, W. Chen, L. Wang, Y. Liu, L. Chen, Cobalt sandwich complex-based covalent organic frameworks for chemical fixation of CO_2, Sci. China Mater. 65 (2022) 1377–1382, https://doi.org/10.1007/s40843-021-1842-8.
[43] Z. Guo, Y. Hu, S. Dong, L. Chen, L. Ma, Y. Zhou, L. Wang, J. Wang, Spring-loaded" mechanism for chemical fixation of carbon dioxide with epoxides, Chem. Catal. 2 (2022) 519–530, https://doi.org/10.1016/j.checat.2021.12.023.
[44] Z. Fang, Z. Deng, X. Wan, Z. Li, X. Ma, S. Hussain, Z. Ye, X. Peng, Keggin-type polyoxometalates molecularly loaded in Zr-ferrocene metal organic framework nanosheets for solar-driven CO_2 cycloaddition, Appl. Catal. B 296 (2021) 120329, https://doi.org/10.1016/j.apcatb.2021.120329.
[45] Y. Li, J. Zhang, K. Zuo, Z. Li, Y. Wang, H. Hu, C. Zeng, H. Xu, B. Wang, Y. Gao, Covalent Organic Frameworks for Simultaneous CO_2 Capture and Selective Catalytic Transformation, Catalysts 11 (2021) 1133, https://doi.org/10.3390/catal11091133.
[46] Q. Yang, H. Peng, Q. Zhang, X. Qian, X. Chen, X. Tang, S. Dai, J. Zhao, K. Jiang, Q. Yang, J. Sun, L. Zhang, N. Zhang, H. Gao, Z. Lu, L. Chen, Atomically Dispersed High-Density Al–N_4 Sites in Porous Carbon for Efficient Photodriven CO_2 Cycloaddition, Adv. Mater. 33 (2021) 2103186, https://doi.org/10.1002/adma.202103186.
[47] X. Fang, L. Yang, Z. Dai, D. Cong, D. Zheng, T. Yu, R. Tu, S. Zhai, J. Yang, F. Song, H. Wu, W. Deng, C. Liu, Poly(ionic liquid)s for Photo-Driven CO_2 Cycloaddition: Electron Donor–Acceptor Segments Matter, Adv. Sci. 10 (2023) 2206687, https://doi.org/10.1002/advs.202206687.
[48] Y. Guo, W. Chen, L. Feng, Y. Fan, J. Liang, X. Wang, X. Zhang, Greenery-inspired nanoengineering of bamboo-like hierarchical porous nanotubes with spatially organized bifunctionalities for synergistic photothermal catalytic CO_2 fixation, J. Mater. Chem. A 10 (2022) 12418–12428, https://doi.org/10.1039/D2TA02885A.
[49] C. Huang, J. Dong, W. Sun, Z. Xue, J. Ma, L. Zheng, C. Liu, X. Li, K. Zhou, X. Qiao, Q. Song, W. Ma, L. Zhang, Z. Lin, T. Wang, Coordination mode engineering in stacked-nanosheet metal–organic frameworks to enhance catalytic reactivity and structural robustness, Nat. Commun. 10 (2019) 2779, https://doi.org/10.1038/s41467-019-10547-9.
[50] Y. Zhi, P. Shao, X. Feng, H. Xia, Y. Zhang, Z. Shi, Y. Mu, X. Liu, Covalent organic frameworks: efficient, metal-free, heterogeneous organocatalysts for chemical fixation of CO_2 under mild conditions, J. Mater. Chem. A 6 (2018) 374–382, https://doi.org/10.1039/C7TA08629F.